ACS Catalysis

Research Article

pubs.acs.org/acscatalysis

Investigation of Selective Catalytic Reduction of N_2O by NH_3 over an Fe−Mordenite Catalyst: Reaction Mechanism and O_2 Effect

Xinyan Zhang,[†] Qun Shen,[†] Chi He,[†] Chunyan Ma,[†] Jie Cheng,[†] Landong Li,[‡,*] and Zhengping Hao[†,*]

[†]Department of Environmental Nano-materials, Research Center for Eco-Environmental Sciences, Chinese Academy of Sciences, Beijing 100085, P. R. China

[‡]Key Laboratory of Advanced Energy Materials Chemistry (Ministry of Education), College of Chemistry, Nankai University, Tianjin 300071, P.R. China

Supporting Information

ABSTRACT: We systematically investigated the reaction mechanism and effect of O_2 on N_2O reduction by NH_3 over an Fe−Mordenite (MOR) catalyst. O_2 has no inhibitory effect on N_2O reduction, and NH_3 selective catalytic reduction (SCR) of N_2O is superior to NH_3 oxidation by O_2. We found that the mechanism of NH_3 SCR of N_2O involves the redox cycle of Fe(III)−OH sites, with Fe(III)−OH reduction by NH_3 as the first and rate-determining step. Then N_2O is activated at the reduced Fe(II)−OH sites into NO/N or N_2/O, reoxidizing the Fe(II)−OH into Fe(III)−OH sites. Next, the NO formed in situ reacts with adsorbed NH_2 to form NH_2NO, which further decomposes to N_2 and water. In addition, some NO may join with O to form NO_2, which reacts with NH_4^+ to produce NH_4NO_2 and further decomposes to N_2 and water. It is possible that under the steady state, N−NO breaking accounts for two-thirds of N_2O splitting. The formation of NO intermediates plays a crucial role in this reaction. The structural arrangement of MOR zeolites and the high content of Fe ions provides two proximal Fe ions, that is, Fe(III)···Fe(III) pairs, as the active sites for this N−NO breaking, resulting in the high activity of Fe−MOR.

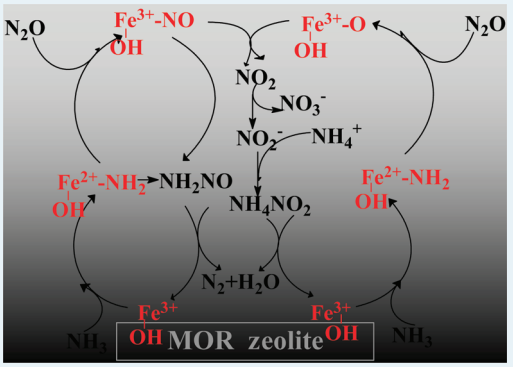

KEYWORDS: *Fe−MOR catalyst, N_2O, O_2 effect, NH_3 SCR, mechanism*

1. INTRODUCTION

Although nitrous oxide (N_2O) has generally been considered a relatively harmless gas, it has recently been shown to be harmful to the environment because it contributes to the greenhouse effect and ozone layer depletion.[1−3] Moreover, the atmospheric N_2O concentration is increasing by about 0.5−0.9 ppb per volume per year, and this increase is mainly caused by human activities, with manufacturing exhaust of compounds such as adipic and nitric acid being a particularly important source.[2,3] Therefore, extensive efforts have been devoted to developing effective technologies to control N_2O emission from these sources. The simplest control technology for N_2O release is based on the catalytic decomposition of N_2O to N_2 and O_2. Fe−zeolites are cost-effective and efficient because of their strong N_2O decomposition activities and high stability, even in the presence of O_2, NO, H_2O, and SO_2.[3] However, Fe−zeolites are not sufficient when applied to the removal of N_2O from nitric acid (HNO_3) plants containing both high N_2O concentrations and low temperatures in the tail gases (usually below 725 K), since the highest N_2O conversion obtained is below 80% under industrial conditions.[4] The decomposition of N_2O over Fe−zeolites can be facilitated by the addition of a reductant, such as hydrocarbon, ammonia (NH_3), or carbon monoxide. When NH_3 functions as a reducing agent, the N_2O conversion is increased, and NO and N_2O are simultaneously reduced in the presence of O_2 at low temperatures.[5−7] Moreover, the N_2O reduction by NH_3 can be promoted by NO, as reported similarly on N_2O decomposition.[8−10] Alternatively, N_2O reduction is inhibited by NO and O_2 in the presence of other reductants.[11,12] In addition, NH_3 is readily available in HNO_3 production. Therefore, NH_3-selective catalytic reduction (SCR) of N_2O seems to be the most promising technology for N_2O reduction from HNO_3 tail gases.

Although several studies have examined the process of NH_3 SCR of N_2O, the specific mechanism of N_2O reduction is still unclear. Moreover, the role of O_2 in the reduction process is also dependent on the catalysts used. The promotion effect of NH_3 in the reduction of N_2O was first reported over a Co/MgO catalyst.[13] It was suggested that NH_3 adsorbed on the Mg−O site reacts with the surface oxygen and releases the active site. The N_2O reduction process is inhibited by O_2 because the reductant NH_3 prefers to react with O_2. Most studies on NH_3 SCR of N_2O have focused on Fe-exchanged zeolites, especially Fe−BEA catalysts.[5−7] The reduction of N_2O by NH_3 obeys a Mars and Van Krevelen mechanism involving a redox cycle of $Fe^{3+} \leftrightarrow Fe^{2+}$. N_2O decomposes into O* surface

Received: November 2, 2011
Revised: February 19, 2012
Published: February 21, 2012

 © 2012 American Chemical Society

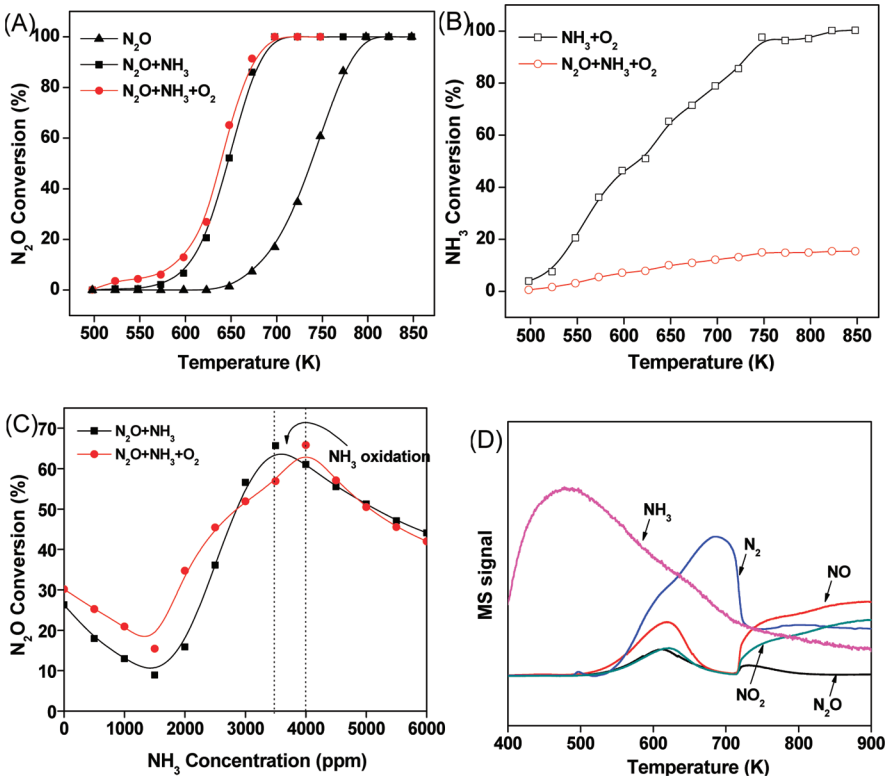

Figure 1. (A) N_2O conversion in direct decomposition and reduction by NH_3 over Fe−MOR. (B) NH_3 conversion for NH_3 oxidation by O_2 in the presence and absence of N_2O. (C) Conversion of N_2O by NH_3 as a function of $P(NH_3)$ in the presence and absence of O_2. (D) Temperature-programmed surface reaction (TPSR) profiles of NH_3 oxidation with O_2. Conditions: 0.1 g catalyst, 5000 ppm N_2O, 0 or 4000 ppm NH_3, 0 or 5% O_2, and the balance He. GHSV = 30 000 h^{-1}.

species on specific reduced Fe sites with the concurrent release of N_2. These O* species do not compete with O* originating from O_2 for their removal by NH_3. Therefore, O_2 has no inhibitory effect on N_2O reduction by NH_3. Recently, Louis-Rose et al.[14] reported the NH_3 SCR of N_2O on polycrystalline Cu planar chips and found that N_2O reduction requires copper in its metallic state; the presence of oxygen (at lower concentrations than NH_3) leads to more efficient NH_3 oxidation, since O_2 is more active with NH_3 than N_2O.[11]

Although it is generally believed that different oxygen species are generated by O_2 and N_2O, and both could react with NH_3, the role of different oxygen species in the reduction reaction as well as the reaction mechanism of NH_3 SCR has not been studied in detail. Moreover, most studies have focused on the interference of NH_3 and other components, such as NO and O_2, by studying the kinetics of the reaction. There are no reports of the activation mechanism of N_2O and NH_3 over Fe−zeolites. This information would be very useful in developing an improved process for N_2O reduction by NH_3 over Fe−zeolites. In our previous study, we found that N_2O SCR by NH_3 over an Fe−Mordenite (MOR) zeolite effectively eliminates N_2O and exhibits high activity and excellent stability under practical conditions.[15] Therefore, in this study, the role of different oxygen species generated by O_2 and N_2O, as well as the reaction mechanism of NH_3 SCR, was studied in detail over the Fe−MOR catalyst. Temperature-programmed reduction or oxidation experiments and in situ diffuse reflectance infrared Fourier transform spectroscopy (DRIFTS) were used to clarify the possible reaction pathways and mechanisms.

2. EXPERIMENTAL METHODS

2.1. Catalyst Preparation. The catalyst used in this study was Fe−MOR prepared by ion exchange of 5.0 g of H−MOR (Sinopec Co., Si/Al ≈ 12) with 0.05 M $FeCl_3$ solution at room temperature. After ion exchange, the sample was washed thoroughly with deionized water, dried at 373 K, and calcined at 873 K for 4 h.

2.2. Activity Measurements. N_2O and NH_3 conversion experiments were performed in a fixed-bed flow microreactor at ambient pressure. In each run, 0.1 g of catalyst (40−60 mesh) was placed in a quartz reactor (4 mm i.d.) and pretreated in a He stream at 873 K for 1 h. After the reactor was cooled to 523 K, the reactant gas mixture (5000 ppm of N_2O, with/without 4000 ppm of NH_3, with/without 5% O_2; He balance) was fed to the reactor. The total flow rate of the mixed gases was set at 60 mL/min (GHSV = 30 000 h^{-1}). Next, the temperature was increased from 500 to 850 K at 25 K intervals (maintained for 20 min at each temperature point) to obtain steady-state N_2O and NH_3 conversion. The outlet gas composition was analyzed online using a quadrupole mass spectrometer (Omnistar Thermostar). Eight mass characteristics of NO (30), NO_2 (30, 46), N_2O (28, 30, 44), N_2 (28), NH_3 (17, 18), H_2O (17, 18), O_2 (32), and He (4) were followed. The intensities of NH_3 (17), H_2O (18), N_2 (28), and NO (30) were determined by solving a linear system of equations.

The kinetic studies of N_2O reduction by NH_3 as a function of NH_3 concentration ($P(NH_3)$, ppm) in the presence and absence of O_2 were performed at a steady state (T = 650 K), and a constant space velocity (GHSV = 30 000 h^{-1}). The N_2O and O_2 concentrations (if present) in the feed were 2500 ppm

dx.doi.org/10.1021/cs200568w | ACS Catal. 2012, 2, 512−520

and 5%, respectively, with NH_3 concentrations varying between 0 and 6000 ppm.

Temperature-programmed oxidation (TPO) by N_2O was performed after activation of Fe−MOR in H_2/He (10/90 v/v) at 773 K. N_2O (30 mL, 2/98 v/v) was fed to the reactor, and the temperature was increased from 500 to 850 K. Temperature-programmed reduction (TPR) by NH_3 was performed after oxidation by N_2O (2/98 v/v) at 773 K of Fe−MOR, which was previously reduced by H_2/He (10/90 v/v) at 773 K. Next, 30 mL of NH_3 (2/98 v/v) was fed to the reactor, and the temperature was increased from 500 to 850 K.

2.3. O_2/N_2O Temperature-Programmed Desorption (O_2-TPD/N_2O-TPD). O_2 temperature programmed desorption (TPD) and N_2O-TPD of Fe−MOR after activation under various conditions were conducted on a Micromeritics Chemisorb 2720 apparatus. Prior to the TPD run, the Fe−MOR catalyst was pretreated in an O_2/Ar (10/90 v/v) stream at 773 K or a N_2O/He (2/98 v/v) stream at 773 K for 0.5 h and then cooled to room temperature in the same gas after reduction at 773 K in H_2/He (10/90 v/v). Afterward, the sample was heated at a rate of 10 K/min^{-1} to 1250 K in a He stream. The effluent gas composition was analyzed online with a TCD detector facilitated by mass spectroscopy coupling when necessary.

2.4. Fourier Transform Infrared (FTIR) Spectroscopy Studies. In situ DRIFTS spectra were collected on the spectrometer (BrukerTensor27) with 256 scans at a resolution of 4 cm^{-1}. A self-supporting pellet (∼50 mg) consisting of the catalyst sample was placed in the IR flow cell and treated at 673 K in a He flow of 30 mL for 0.5 h after calcination in air at 873K for 4 h. Next, the cell was cooled to room temperature. The background spectrum was taken in flowing He at specific temperatures, and these values were subtracted from the sample spectrum obtained at the same temperatures.

After the He stream was switched to a mixture of various gases, a series of temperature-dependent FTIR spectra on the zeolite catalyst were sequentially recorded (with each temperature point maintained for 30 min).

3. RESULTS

3.1. Physical Characterization of the Fe−MOR Zeolite Catalyst. The prepared Fe−MOR catalyst contained 2.68% Fe, with an Fe/Al ratio of 0.32, and a specific surface area of 478 m^2 g^{-1}, similar to that of the parent H−MOR zeolite. After loading of the Fe species, the zeolite structure was well preserved, as shown by the XRD results. The nature and distribution of Fe species in MOR, as previously accessed by UV−vis spectra, are mainly isolated ferric ions and a small amount of iron oxide aggregates. Detailed information about the structure of Fe−MOR can be found in our previous study and related report.[5−7,12,15]

3.2. Catalytic Activity of N_2O Reduction by NH_3 over the Fe−MOR Catalyst. Figure 1 shows the catalytic behavior of N_2O reduction by NH_3 over the Fe−MOR catalyst. As shown in Figure 1A, the reduction of N_2O by NH_3 started at ∼550 K, and 90% N_2O conversion (T_{90}) was reached at ∼680 K. N_2 and H_2O were the only products detected. The onset of N_2O decomposition occurred at ∼650 K, and T_{90} occurred at ∼785 K. Thus, the boosting effect of NH_3 on the reduction of N_2O to N_2 was evident in the decrease of T_{90} by ∼105 K, compared with that of N_2O decomposition.

In its simplest form, the catalytic decomposition of N_2O has been described as follows:

$$N_2O + * \rightarrow N_2 + *\text{-}O \quad \text{(R1)}$$

$$2*\text{-}O \rightarrow O_2 + 2* \quad \text{(R2)}$$

$$N_2O + *\text{-}O \rightarrow N_2 + O_2 + * \quad \text{(R3)}$$

In the presence of NH_3, the surface oxygen can also be removed according to R4:

$$2NH_3 + 3*\text{-}O \rightarrow N_2 + 3H_2O + 3* \quad \text{(R4)}$$

It should be noted that no O_2 is formed during N_2O reduction by NH_3 in the absence of O_2 (Supporting Information Figure S1), and the stoichiometry of the reaction was $N_2O/NH_3 \approx 3/2$. This demonstrates that in the presence of NH_3, N_2O catalytic decomposition proceeding via R1−R3 is significantly inhibited, and N_2O is mainly converted by NH_3 through the global reaction of

$$3N_2O + 2NH_3 \rightarrow 4N_2 + 3H_2O \quad \text{(R5)}$$

This phenomenon differs from the catalytic behavior of methane (CH_4) SCR of N_2O over Fe−zeolite, in which the direct decomposition of N_2O contributes largely to the N_2O conversion in the presence of the CH_4 reductant, as shown in our previous work.[16]

In the presence of O_2, no decrease in N_2O conversion was observed, as shown in Figure 1A. Instead, there was a slight improvement in N_2O conversion under these conditions. This suggests that there is no inhibitory effect of O_2 on the N_2O conversion. The improved N_2O conversion may be related to NH_3 oxidization by O_2, thus changing the NH_3/N_2O stoichiometry, which is supported by the results in Figure 1C. It has been confirmed by our kinetic experiments that the N_2O conversion rate is significantly influenced by the NH_3 content in the flow, which has also been reported in previous studies.[5] As shown in Figure 1C, in the absence of O_2, the N_2O removal rate reaches a maximum value when NH_3 content is ∼3500 ppm. The most favorable ratio of NH_3/N_2O, equaling 2/3 (3500 ppm/5000 ppm), also confirms that the N_2O reduction reaction by NH_3 follows R5. In the presence of excess O_2, the maximum N_2O conversion rate occurs at NH_3 concentrations of ∼4000 ppm, which is similar to the N_2O conversion rate when NH_3 concentrations are ∼3500 ppm in the absence of O_2. This suggests that O_2 does not inhibit N_2O reduction and that even excess O_2 does not efficiently react with NH_3. Moreover, as shown in Figure 1B, the NH_3 oxidation conversion by O_2 in the presence of N_2O is much lower than that in the presence of O_2 alone, strongly suggesting that N_2O SCR by NH_3 is superior to NH_3 oxidation by O_2 in the N_2O +NH_3+O_2 reaction system.

In addition, Figure 1D illustrates that significant amounts of NO, NO_2, and N_2O are formed at different temperatures when NH_3 is oxidized by O_2, but only N_2 is detected as the main product in the N_2O + NH_3 + O_2 reaction system (Supporting Information Figure S2). This suggests that NH_3 could be oxidized by N_2O or O_2; however, N_2O is much more active than O_2, and their reaction pathways are quite different. The high activity of N_2O is similar to those of the unique α-oxygen species generated by N_2O, which are much more active than the O species originating from O_2; this results in the extraordinary oxidizing activity of benzene to phenol.[17] To evaluate the possible role of these different surface oxygen

dx.doi.org/10.1021/cs200568w | ACS Catal. 2012, 2, 512−520

species, TPD experiments of Fe−MOR were conducted after calcination in O_2 or N_2O (Figure 2).

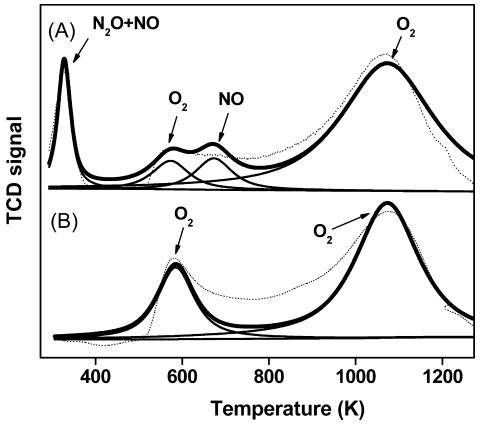

Figure 2. TPD profiles of Fe−MOR activated in N_2O (A) and O_2 (B) at 773 K after reduction in H_2 at 773 K.

3.3. N_2O TPD and O_2 TPD of Reduced Fe−MOR Catalyst. As shown in Figure 2B, after calcination in O_2, there were two broad peaks of O_2 desorption centered at ∼590 and 1100 K. After activation of N_2O, there was still a broad O_2 desorption peak at high temperatures (>800 K), but several other desorption peaks appeared at lower temperatures (Figure 2A). The natures of the desorbing species were identified by mass spectroscopy. The desorption peaks at 380, 580, and 680 K were attributed to N_2O and NO, O_2, and NO, respectively. This indicates that different surface oxygen species exist after N_2O treatment, and one of them desorbs at ∼580 K, which is similar to that seen after O_2 treatment. It is possible that this surface oxygen is analogous to the α-oxygen that forms by the interaction of N_2O with Fe−ZSM-5 zeolite.[17] However, α-oxygen is thought to be associated with binuclear Fe complexes rather than with isolated atoms.[18] Moreover, the desorbing temperature (∼580 K) of these oxygen species over Fe−MOR after N_2O treatment is close to the O_2 desorption temperature (∼590 K) after calcination in O_2, indicating that this species does not resemble the unique α-oxygen deposited only by N_2O on Fe^{2+} and that the nature and activity of these oxygen species deposited by N_2O on Fe−MOR are similar to those of the oxygen deposited by O_2.

Surprisingly, NO desorption was observed at 380 and 680 K, suggesting that a reaction occurs that can be described stoichiometrically as

$$2N_2O \rightarrow 2NO + N_2 \qquad \text{(R6)}$$

This occurs by breaking the much stronger N−NO bond (481 kJ mol^{-1}), rather than the weaker NN−O bond (167 kJ mol^{-1}). This reaction was recently demonstrated during the decomposition of N_2O on Ba/MgO[19] and Fe−FER.[20] The NO desorption at ∼610 K has also been identified in the TPD of Fe−ZSM-5 after exposure to N_2O at 417 K.[21] It has also been found when N_2O interacts at room temperature with Fe(II) species in both Fe−MCM-41 and Fe−ZSM-5.[22] In our study, significant amounts of NO desorbed at 380 and 610 K, indicating that NO could form through R6 and play a role in the N_2O SCR reaction. However, during the reaction, NO easily reacted with NH_3, as reported in our previous studies,[5,12] but could not be identified (Figure S1). Therefore, its role in the N_2O SCR reaction is difficult to determine.

To verify the NO generation mechanism and its contribution, the reaction rate was reduced by lowering the N_2O concentration, and the N_2O-pulse experiment was conducted at temperatures ranging from 373 to 773 K (Figure S3). The results revealed that O_2, N_2, and NO formed at every temperature. More interestingly, the N_2 concentration was greater than that of O_2, that is, the ratio of N_2/O_2 at every temperature point (3.5−4:1) was greater than the stoichiometric ratio of R1 (2:1). Moreover, the ratio of NO/N_2 was roughly 1:1, which is lower than the stoichiometric ratio of R6 (2:1). Relating these ratios to R1 and R6, it could be roughly estimated that N_2O activation is split equally by R1 and R6 (50% for each reaction). Multiple N_2O splitting through R1 and R6 has also been reported on Fe−BEA, and the roles of these reactions were estimated by reaction of $^{14}N_2O$ with $^{15}NH_3$. However, during N_2O reduction, the role of R6 over Fe−BEA accounts for only 2% of the complete $N_2O + NH_3$ reaction, suggesting that N_2O reacts with NH_3 mainly through O species over Fe−BEA.[23] Thus, the activation mechanism of N_2O is different for Fe−MOR and Fe−BEA, the most common catalysts for N_2O SCR by NH_3. The stronger N−NO breaking of N_2O over Fe−MOR may be related to its much higher activity for NH_3 SCR.

3.4. FTIR Study of the Activation Mechanism of NH_3 and N_2O. The intermediate species of NH_3 and N_2O activation and their reaction were studied in detail using DRIFTS to clarify the possible reaction pathways and mechanisms.

3.4.1. FTIR Spectra of NH_3 Adsorption on Fe−MOR. Figure S4 shows FTIR spectra of Fe−MOR collected at different temperatures in the He stream. Three peaks (3740, 3670, and 3620 cm^{-1}) were observed and assigned to the OH stretching mode. The peaks at 3740 and 3620 cm^{-1} could be assigned to the OH stretching mode of the terminal silanols (Si−OH) and bridging OH groups (i.e., Brønsted acidic site, Si−OH(Al) of MOR zeolite), whereas the peak at 3670 cm^{-1} could be assigned to the OH group on Fe^{3+} species, which has been demonstrated with an Fe−BEA catalyst.[24]

Figure 3 presents the FTIR spectra of Fe−MOR during the adsorption and desorption of NH_3. After the sample was treated with NH_3 at room temperature, the OH stretching bands at 3670 cm^{-1} were consumed, indicating that NH_3 was adsorbed on the Fe−OH. With increasing temperatures, the band at 3620 cm^{-1} was consumed, and the intensity of the consumed band at 3670 cm^{-1} decreased. This indicates that NH_3 could be adsorbed on the Fe−OH and, at higher temperatures, on the bridging OH groups. After NH_3 adsorption at room temperature, new NH_3 adsorbed species bands were observed at 3290, 3050, 2800, 1632, 1470, and 1246 cm^{-1}.

The bands at 1246 and 1470 cm^{-1} were assigned to the adsorption of NH_3 on the Lewis acid sites (asymmetric bending vibration of the N−H bonds in coordinated NH_3) and NH_3 coordinated on the Brønsted acidic site (NH_4^+), respectively.[25,26] Furthermore, the broad band at 3400−3100 cm^{-1} could be assigned to the stretching mode of N−H. The bands at 3353 and 3290 cm^{-1} were ascribed to NH_4^+ ions with three hydrogen atoms bonded to three oxygen ions of the AlO_4 tetrahedral structure (3H structure), and the bands at 3050 and 2795 cm^{-1} were due to the NH_4^+ ions with two hydrogen atoms bonded to three oxygen ions of the AlO_4 tetrahedral structure (2H structure).[25,26] The band intensities decreased gradually with increasing temperature. With increasing temperature, the NH_3 bands coordinated on the Brønsted acidic sites

dx.doi.org/10.1021/cs200568w | ACS Catal. 2012, 2, 512−520

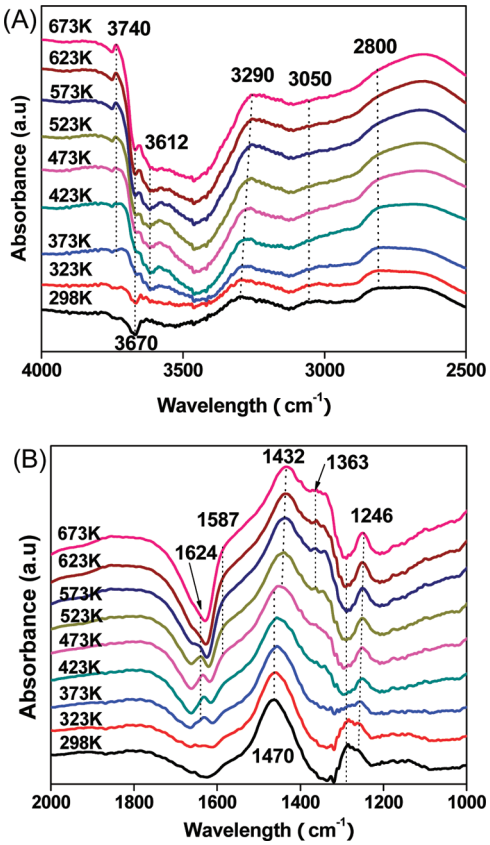

Figure 3. FTIR spectra of Fe−MOR taken after adsorption of NH_3 (4000 ppm) at room temperature, followed by purging with He for 30 min and successive heating in He at various temperatures.

disappeared, and the intensity of the bands ascribed to NH_3 adsorbed on the Lewis acid sites remained the same. This desorption sequence coincides with the expected adsorption strength of these adsorption species.

The NH_3 coordinated on the Brønsted acidic sites was weaker than that on the Lewis acid sites. Desorption of the unreacted NH_3 and activation of NH_3 was responsible for these decreases. A new weak band was visible at 1624 cm^{-1} from 373 to 573 K but vanished at temperatures above 573 K. The assignment of this new peak is discussed in the following section. With increasing temperatures, intensities of the three bands at 1587, 1432, and 1363 cm^{-1} increased, following a decrease in the bands assignable to NH_3. The bands at 1587 and 1363 cm^{-1} were assigned to amide ($-NH_2$) scissorings and ($-NH_2$) waggings, respectively.[27−29] The band at 1432 cm^{-1} was ascribed to −NH deformation modes.[27] This indicates that upon heating, the adsorbed NH_3 could be activated to form $-NH_2$ and −NH intermediates through abstraction of hydrogen.

3.4.2. FTIR Spectra of N_2O Adsorption on Fe−MOR. Figure 4 shows the FTIR spectra of Fe−MOR during the adsorption and desorption of N_2O. After the sample was treated with N_2O at room temperature, the OH stretching bands at 3670 cm^{-1} were consumed, indicating that N_2O was adsorbed on the Fe−OH sites. With increasing temperatures, the band at 3670 cm^{-1} was recovered while the intensity of the consumed band at 3620 cm^{-1} was not changed. This indicates that N_2O is mainly activated at the Fe−OH sites. In addition, several new bands for N_2O adsorbed species at 2232, 2208, 1846, 1624, 1426, 1354,

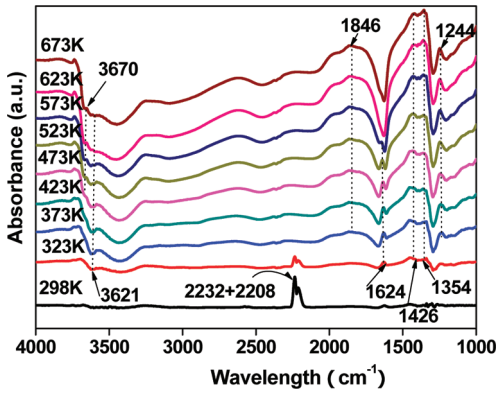

Figure 4. FTIR spectra of Fe−MOR taken after adsorption of N_2O (5000 ppm) at room temperature, followed by purging with He for 30 min and successive heating in He at various temperatures.

and 1244 cm^{-1} were observed when the reaction temperature increased.

The band at 2232 and 2208 cm^{-1} could be assigned to adsorbed N_2O, and these bands disappeared at temperatures above 373 K. This weak adsorption property of N_2O over the Fe−MOR catalyst is demonstrated by the N_2O-TPD results and has also been reported on the surface of Cu(110).[14] On the other hand, new N_2O dissociation species have been identified upon heating. The band appearing at 1846 cm^{-1} at temperatures above 373 K could be assigned to NO adsorbed on the Fe^{3+} ions. The band at 1244 cm^{-1} could be assigned to NO_2^-, and the bands at 1354 and 1426 cm^{-1} could be assigned to the NO_3^- species.[26,27] This indicates that upon heating, adsorbed N_2O could be dissociated to NO and adsorbed as nitrate and nitrite ad-species on Fe−MOR.

Interestingly, the band at 1624 cm^{-1} appeared at room temperature and disappeared at temperatures above 573 K. Similar bands were observed for NH_3 adsorption at temperatures from 373 to 573 K (Figure 3). The band located at this position has been previously assigned to adsorbed NO_2[29] and bridging nitrates,[30−33] or the asymmetric deformation modes of NH_3 coordinated on the Lewis acid sites.[25] For N_2O activation, the other HNO_3 species' bands (1354 and 1426 cm^{-1}) did not change upon heating from room temperature to 658 K. Thus, they may not be the same species. We assigned this band to adsorbed NO_2 species. This NO_2 adsorbed species likely formed through NO oxidization with the O^- atom, or with lattice oxygen (O^{2-}), in the absence of O_2. As shown in N_2O-TPD, N_2O could be activated to NO and O_2, which react with each other to form NO_2. However, NO_2 has never been identified from the N_2O-TPD results with only NO and O_2 detected, possibly because it is at such low concentrations or has very high reactivities. To confirm our assignments, we performed NO_2-TPD (Figure S5) and examined the FTIR spectra of NO adsorption (Figure 5). As shown in Figure S5, the adsorbed NO_2 was desorbed at 530 K and further decomposed to NO and O_2. This could explain the complete disappearance of adsorbed NO_2 at temperatures above 573 K in the FTIR spectra. In addition, the NO adsorption FTIR spectra clearly showed adsorbed NO and NO_2 on Fe−MOR.

For NH_3 adsorption, we ascribed it (band at 1624 cm^{-1}) to the HNO_3 species, since NO adsorption (to form NO_2) was not observed. In addition, the other NH_3 bands coordinated on Lewis acid sites (1246 cm^{-1}) did not show the same trends upon heating. The N_2O species formed from NH_3 activation in

dx.doi.org/10.1021/cs200568w | ACS Catal. 2012, 2, 512−520

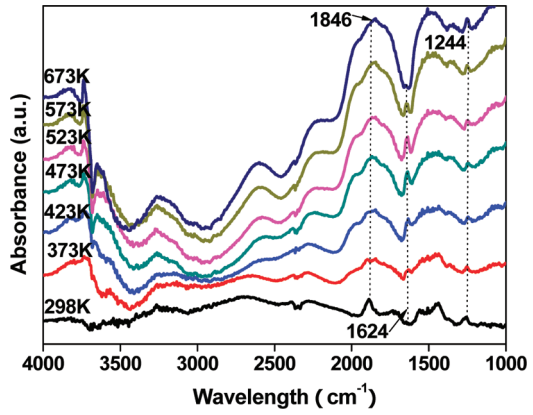

Figure 5. FTIR spectra of Fe−MOR taken after adsorption of NO (1%) at room temperature, followed by purging with He for 30 min and successive heating in He at various temperatures.

the absence of O_2 have been reported previously on CuO−TiO_2, possibly through the NH reaction with O^{2-}.[23] In our case, the intermediate NH may react with O^{2-} to form NO_2^-, which further reacts with OH to form nitrates. These HNO_3 species form at 373 K, and NH_3 dissociation confirmed that these species form through oxidation of intermediate NH and a further reaction with OH. For N_2O activation, the band for NO_2 species is present at room temperature when NO is already present.

3.4.3. FTIR Study of the Interaction of N_2O with NH_3. The NH_3 SCR of the N_2O mechanism with respect to the behavior of activated NH_3, N_2O, and the NH_3 + N_2O interaction on the surface of Fe−MOR catalyst, was studied using in situ FTIR, as shown in Figure 6.

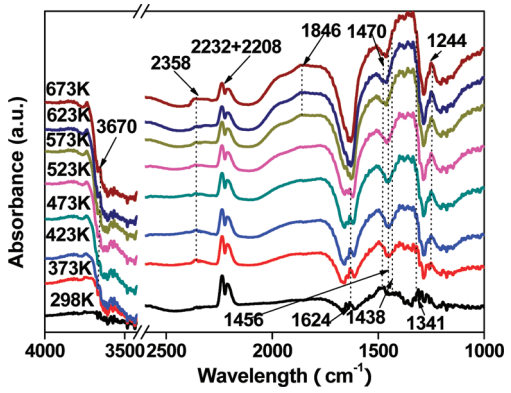

Figure 6. FTIR spectra of Fe−MOR treated with a flow of 5000 ppm N_2O + 4000 ppm NH_3 at various temperatures.

After the sample was treated with N_2O and NH_3 at room temperature, the OH stretching band at 3670 cm^{-1} was first consumed and then recovered at increased temperatures, indicating that the N_2O + NH_3 reaction proceeds on the Fe−OH sites. The intensity of the consumed band at 3620 cm^{-1} was not changed, and the NH_3 bands coordinated on the Brønsted acidic sites (1470 cm^{-1}) greatly decreased at temperatures above 373 K, while the intensity of the band ascribed to NH_3 on the Lewis acid sites (1243 cm^{-1}) was almost unchanged. This confirms that both N_2O and NH_3 are adsorbed and activated on the Fe−OH sites. Upon heating, with decreased adsorption of N_2O and NH_3, new adsorbed species, such as −NH (1456 cm^{-1}), NO (1846 cm^{-1}), nitrate, and NO_2 ad species (1624 cm^{-1}) were observed. It should be noted that the NH_3 activation species NH_2 disappeared during the N_2O and NH_3 reaction, suggesting that NH_2 formation is the rate-determining step. NH_2 reacts with NO to form NH_2NO and is further converted to N_2 and H_2O. The latter reaction is very active, as follows the NH_3 SCR reaction.

3.5. N_2O TPO and NH_3 TPR Experiments. The above results suggest that NH_3 and N_2O could be adsorbed and activated at the Fe ions site and form NH_x, NO_x, or O intermediate species at different temperatures to react with each other. The redox cycle of "Fe ions", which involves the activation on Fe ion sites with N_2O and NH_3 as an oxidant and reductant, respectively, and further interaction between these intermediates determine the reaction process. Therefore, temperature-programmed reduction and oxidation experiments were performed to obtain information on the redox mechanism and reactivity of these intermediate species. In these experiments, the nature of the released gases was analyzed online by mass spectroscopy detection. TPO by N_2O was conducted after reduction by H_2 at 773 K, instead of NH_3, because NH_3 adsorbed too strongly on the catalyst and would ultimately desorb. This would alter the results, since the NH_3 + N_2O reaction supersedes the oxidation of reduced Fe species by N_2O. We observed no H_2 consumption when TPR experiments were performed at temperatures up to 773 K after Fe−MOR was reduced by NH_3 at 773 K, as has also been shown previously on an Fe−BEA catalyst.[19] Thus, it is possible that the reduction state of the Fe species is very similar when Fe−MOR is activated at 773 K with NH_3 or H_2.

Therefore, TPO by N_2O was performed after activation of Fe−MOR with H_2 at 773 K, and the results are shown in Figure 7A. The first N_2O consumption occurred at intermediate temperatures (425−650 K), with the release of N_2 only. This may correspond to the specific interaction between N_2O and reduced Fe sites with the anchoring of O* R1. The onset of the second N_2O consumption started at around 750 K and corresponded to the initiation of the catalytic decomposition of N_2O into N_2 and O_2. Surprisingly, no NO_x was found in the TPO process, although it has been identified in the N_2O TPD.

Similar observations have been reported over Fe−BEA catalyst[19] that could be related to the differences in reaction conditions of N_2O-TPD and TPO. In the TPD experiment, the amount of adsorbed NO_x and N_2O were equally low (tens of parts per million). In the TPO experiment, the generated NO_x species were at much lower concentrations than that of N_2O in the flow (2%), whereas in the absence of reductant NH_3, the formation of these less thermodynamically favored species may be inhibited. TPR by NH_3 was performed after the Fe−MOR catalyst was preoxidized by N_2O at 773 K (Figure 7B). During TPR, very strong adsorption of NH_3 resulted in an uninformative concentration profile. In contrast, the release of N_2 was very clear and occurred at a broad peak with shoulders between 475 and 900 K. The expected H_2O release was delayed due to its retention on the MOR zeolite.

Comparison of the TPR by NH_3 and TPO by N_2O profiles shows that the onset of the TPO profile occurs at lower temperatures. It is possible that in the oxido−reduction cycle of Fe, which regulates the reaction N_2O + NH_3, the reduction of the oxidized Fe sites by NH_3 would be the rate-determining step. This mechanism differs from the catalytic process of Fe−BEA, which is determined by N_2O oxidation.[24] This difference may be caused by the different structure of the zeolite channels,

dx.doi.org/10.1021/cs200568w | ACS Catal. 2012, 2, 512−520

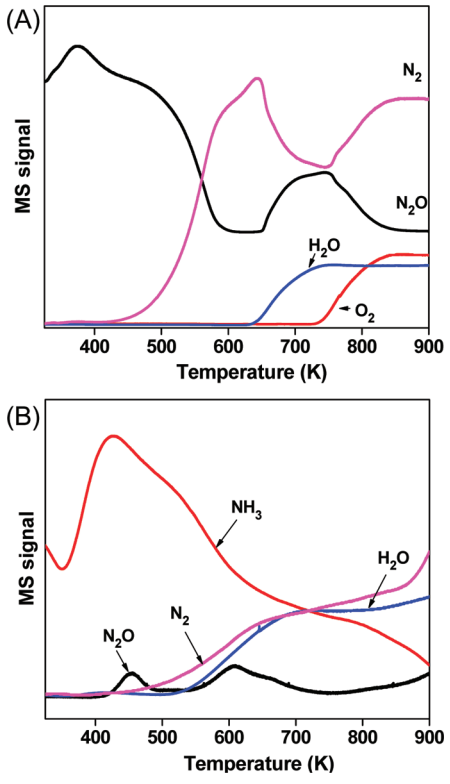

Figure 7. (A) TPO by N_2O of Fe−MOR after reduction in H_2 at 773 K. (B) TPR by NH_3 of Fe−MOR after oxidation in N_2O at 773 K.

since both Fe−BEA and Fe−MOR possess isolated Fe ions as active sites. However, MOR has larger and more open pore channels than BEA, which makes the N_2O dissociation and activation over Fe sites easier on MOR than on BEA, thus making reduction of the oxidized Fe sites by NH_3 the rate-determining step.

The Fe−Fe distance may play an important role in N_2O splitting, since significant NO is formed over the Fe−MOR catalyst, which may require the cooperation of two Fe ions in the neighborhood.[20] To better understand this process and to determine the role of the Fe reduction sites, the TPSR process of N_2O reduction by NH_3 was performed on reduced Fe−MOR, and the results are shown in Figure 8. The SCR reaction

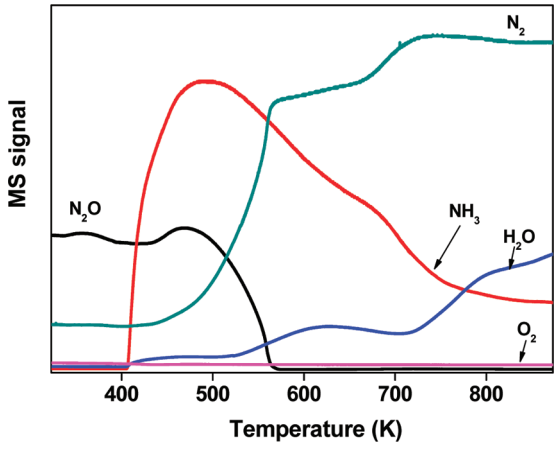

Figure 8. TPSR profiles of N_2O reduction by NH_3 over Fe−MOR after reduction in H_2 at 773 K. Conditions: 0.1 g of catalyst, 5000 ppm N_2O, 4000 ppm NH_3, and the balance He. GHSV = 30 000 h^{-1}.

occurred at much lower temperatures over the previously reduced Fe−MOR than in Figure S1, which confirms that reduction of the oxidized Fe sites by NH_3 is probably the rate-determining step over Fe−MOR.

4. DISCUSSION

4.1. NH_3 and N_2O Activation. As shown in Figure 3, NH_3 could adsorb at the Fe−OH sites (3670 cm^{-1}) and other Brønsted (1470 cm^{-1}) or Lewis acidic sites (1246 cm^{-1}). By increasing the reaction temperature, the intensity of the consumed band of Fe−OH sites at 3670 cm^{-1} was recovered, and the bands of NH_3 coordinated on Brønsted acidic sites disappeared. However, the intensity of the bands ascribed to NH_3 on Lewis acid sites were mostly unchanged. This indicates that the Fe−OH sites and other Brønsted acid sites (1470 cm^{-1}) are the active sites for NH_3 activation and that NH_3 coordinated on Lewis acid sites has no effect on the activity. At increased temperatures, $-NH_2$ (1587 and 1363 cm^{-1}) and −NH (1432 cm^{-1}) intermediates appeared, and the band assigned to adsorbed HNO_3 (1624 cm^{-1}) was observed in the absence of N_2O. Other studies have found that in the absence of oxidized agents, −NH could also interact with lattice oxygen (O_2^-) to produce small quantities of N_2O.[28] However, this reaction would not be sustainable under O_2-free conditions and is not discussed here in detail. Overall, our results (Figure 5) demonstrate that in the absence of N_2O, NH_3 could dehydrogenate to form $-NH_2$ and −NH intermediates through abstraction of hydrogen. The main reaction routes are as follows:

$$NH_3 + OH \rightarrow NH_2 + H_2O \quad \text{(R7)}$$

$$NH_2 + OH \rightarrow NH + H_2O \quad \text{(R8)}$$

$$NH + O_2^- \rightarrow NO_2^- + H \quad \text{(R9)}$$

$$NO_2^- + OH \rightarrow HNO_3 \quad \text{(R10)}$$

With the adsorption of N_2O, the OH stretching band at 3670 cm^{-1} was first consumed and then recovered at increasing temperature, and the intensity of the consumed band at 3620 cm^{-1} was unchanged (Figure 4). This indicates that N_2O was adsorbed and mainly activated on the Fe−OH site, suggesting that both NH_3 and N_2O are adsorbed and activated at the Fe−OH sites. This process is different from that on Fe−BEA, where NH_3 and N_2O interact on separate sites. Adsorbed N_2O was observed at room temperature (2232 and 2208 cm^{-1}) and disappeared at temperatures above 373 K. This weak adsorption property of N_2O over the Fe−MOR catalyst is supported by the N_2O-TPD results and has also been reported over a Cu(110) surface.[14]

On the other hand, new N_2O dissociation species, such as NO_2^- (1244 cm^{-1}), NO_3^- (1354 cm^{-1} and 1426 cm^{-1}), NO (1846 cm^{-1}), and NO_2 (1624 cm^{-1}) were found upon heating. Similarities between the NO-FTIR spectra and the N_2O TPD results suggest that NO is the important N_2O activation intermediate and that NO could further react with O to form NO_2 and other nitrite and nitrate ad-species. This suggests that breaking of the N−NO bond plays an equal or more important role than NN−O breaking (to form O species) in N_2O reduction by NH_3. In addition, the N_2O-pulse results also support the formation of NO at temperatures as low as 373 K. The NH_3 oxidation by O_2 experiments and O_2-TPD results suggest that although O_2 could be activated at almost the same

dx.doi.org/10.1021/cs200568w | ACS Catal. 2012, 2, 512−520

temperature as N_2O to desorb O_2, the activities of O_2 were much lower in the presence of N_2O. This demonstrates that the difference in NH_3 oxidation by N_2O and O_2 lies in the NO formed during N_2O activation, and implies that the N_2O reduction by NH_3 occurred mainly through NO intermediates.

Moreover, the adsorbed NO and O from N_2O activation could react with each other to form adsorbed NO_2 intermediates, as observed in the FTIR spectra and supported by NO_2-TPD (Figure S5). Usually, this NO oxidation to NO_2 is slow over Fe−zeolites;[34] however, a similar finding has also been reported over Fe−ZSM-5 zeolite in the SCR reaction.[35] It is proposed that it is probably the rate-determining step for the standard NH_3 SCR of the NO reaction. Moreover, this process of adsorbed NO accommodated the oxygen deposited by N_2O and facilitates the migration of oxygen through NO_2 intermediates and has been proposed as the possible mechanism for the promoting effect of NO on N_2O decomposition and reduction by NH_3 over Fe−zeolites.[8−10] However, for other process, that is, other reductants, such as hydrocarbon used or over other zolites system, NO mainly adsorbed at the active sites and competed with the N_2O and thus inhibited its decomposition.[11,12]

The main reaction routes of N_2O activation are as follows:

$$N_2O \rightarrow N_2 + O \quad (R1)$$

$$N_2O \rightarrow NO + N \quad (R6)$$

$$NO + O \rightarrow NO_2 \quad (R11)$$

$$NO + OH \rightarrow HNO_2 \quad (R12)$$

$$NO_2 + OH \rightarrow HNO_3 \quad (R13)$$

4.2. Interaction of NH_3 with N_2O. As shown in Figure 6, after the sample was treated with N_2O and NH_3 at room temperature, the OH stretching band at 3670 cm^{-1} was first consumed and subsequently recovered at increased temperatures, while the intensity of the consumed band at 3620 cm^{-1} was unchanged. This confirms that both N_2O and NH_3 are activated at the Fe−OH sites. Upon heating, there is a decrease in adsorbed N_2O, NH_3, −NH (1456 cm^{-1}), NO (1859 cm^{-1}), nitrate, and NO_2 ad-species (1624 cm^{-1}). These results corroborate our above results that NH_3 SCR of N_2O reacts mainly through $-NH_2$ and NO intermediates. The reaction likely proceeds through the following steps, as shown in Figure 9.

First, NH_3 is adsorbed on the Fe(III)−OH sites, followed by reduction of Fe(III)−OH to Fe(II)−OH and formation of adsorbed NH_2. Then N_2O is activated at the reduced Fe(II)−OH into NO/N or N_2/O, and Fe(II)−OH is oxidized into Fe(III)−OH sites. Next, NO reacts with adsorbed NH_2 to form NH_2NO, which further decomposes to N_2 and water; or NO can cooperate with O to form NO_2 intermediate and nitrite ad-species, which react with NH_4^+ to produce NH_4NO_2 and further decompose to N_2 and water. Those reactions of NO with NH_3 follow the typical SCR mechanism ($NO + NH_3 + (1/4)O_2 \rightarrow N_2 + (3/2)H_2O$), which has been proved to proceed quickly at Fe−MOR and other Fe−zeolites.[12,34−36] Since the stoichiometry of the reaction was $N_2O/NH_3 \approx 3/2$ with no other product formed during the steady state reaction and O_2 has no influence on this reaction, the overall reaction at the steady state likely follows a combination of the four reactions: 2/3 of N_2O were activated by $N_2O \rightarrow NO + N$ (a) and 1/3 by $N_2O \rightarrow N_2 + O$ (b), and the formed NO and O_2 react with NH_3 following a typical SCR mechanism ($NO + NH_3 + (1/4)O_2 \rightarrow N_2 + (3/2)H_2O$).

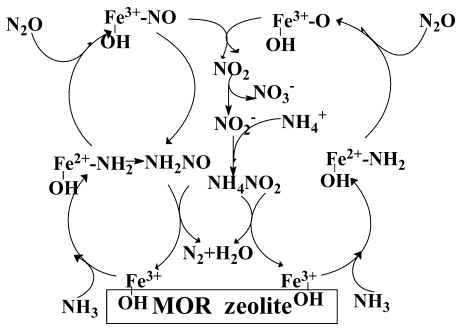

Figure 9. Proposed reaction scheme for the N_2O reduction by NH_3.

$$NH_3 + OH \rightarrow NH_2 + H_2O \quad (R7)$$

$$N_2O \rightarrow N_2 + O \quad (R1)$$

$$2N_2O \rightarrow 2NO + N_2 \quad (R6)$$

$$NH_2 + NO \rightarrow NH_2NO \rightarrow N_2 + OH_2 \quad (R14)$$

$$NO + O \rightarrow NO_2 \quad (R11)$$

$$O^{2-} + 2NO_2 \leftrightarrow NO_2^- + NO_3^- \quad (R15)$$

$$NH_4^+ + NO_2^- \rightarrow NH_4NO_2 \rightarrow NH_2NO + H_2O \rightarrow N_2 + H_2O \quad (R16)$$

On the basis of the above FTIR observations and TPO/TPD reaction, it is likely that 2/3 of the N_2O is activated through this N−NO splitting mechanism and then plays an important role in the NH_3 SCR process over Fe−MOR, which is different from the N_2O splitting mechanism over Fe−BEA (mainly NN−O splitting). In addition, the rate-determining step over Fe−MOR is reduction of Fe(III)−OH by NH_3, whereas for Fe−BEA, it is N_2O oxidation of Fe(II)−OH. These findings all imply that different mechanisms or different active sites may exist in the Fe−MOR zeolite. As proposed for Fe−FER, to achieve this N−NO splitting, the cooperation of two Fe active sites is required.[16] It is likely that an Fe−NNO complex is formed, and the other site attracts the oxygen atom of the Fe−NNO complex to form Fe−O species. Therefore, the strength of N−NO is reduced and broken. To attain this N_2O splitting through the mutual action of two adjacent Fe ions, a suitable distance and enough Fe sites are required. Our previous studies have shown that MOR possesses the superstructure arrangement to host two collaborating Co ions in Co···Co pairs and contributes to its high activity for N_2O decomposition. Taking into account the high Fe ion content in the Fe−MOR and the super structure of MOR, this N−NO splitting of N_2O by cooperation of two close Fe ions is very likely. This could explain the higher activity of Fe−MOR relative to that of Fe−BEA for N_2O reduction with isolated Fe ions as active sites and confirms that these unique Fe(III)···Fe(III) sites in MOR function as active sites that are very important for this reaction.

4. CONCLUSIONS

In this study, the reaction mechanism of N_2O reduction by NH_3 was systematically investigated over an Fe−MOR catalyst.

dx.doi.org/10.1021/cs200568w | ACS Catal. 2012, 2, 512−520

We examined the role of different oxygen species generated by O_2 and N_2O on the catalytic activities. The first step of the reaction is the adsorption of NH_3 on Fe(III)−OH sites, followed by the reduction of Fe(III)−OH to Fe(II)−OH and the formation of adsorbed NH_2. The reduction of Fe(III)−OH and formation of adsorbed NH_2 is the rate-determining step for this reaction. Second, N_2O is activated at the reduced Fe(II)−OH sites into NO/N or N_2/O, and the Fe(II)−OH is reoxidized into Fe(III)−OH sites. Afterward, NO reacts with adsorbed NH_2 to form NH_2NO, which further decomposes to N_2 and water. Further, some NO may cooperate with O to form NO_2, which reacts with NH_4^+ to produce NH_4NO_2 and further decomposes to N_2 and water. It is likely that under the steady state, the ratio of N_2O split by N−NO and NN−O breaking is ∼2:1. Next, NO and O_2 react together with NH_3 following a typical SCR mechanism. Therefore, O_2 alone is much less efficient than N_2O for reacting with NH_3, and O_2 has no influence on the reduction reaction. N−NO splitting of N_2O and the formation of NO intermediates are very important, and two proximal Fe ions, that is, Fe(III)···Fe(III) sites, function as the active sites for this reaction.

■ ASSOCIATED CONTENT

Supporting Information

Additional information as noted in text. This material is available free of charge via the Internet at http://pubs.acs.org.

■ AUTHOR INFORMATION

Corresponding Author

*(L.L.) Phone/Fax: +86-22-2350-0341. E-mail: lild@nankai.edu.cn. (Z.H.): Phone/Fax: +86-10-62923564. Email: zpinghao@rcees.ac.cn.

Notes

The authors declare no competing financial interest.

■ ACKNOWLEDGMENTS

This work was financially supported by National Natural Science Funds for Distinguished Young Scholar (20725723) and National Basic Research Program of China (2010CB732300).

■ REFERENCES

(1) Li, Y.; Armor, J. N. *Appl. Catal., B* **1992**, *1*, L21−L29.
(2) Pérez-Ramírez, J.; Overeijnder, J.; Kapteijn, F.; Moulijn, J. A. *Appl. Catal., B* **1999**, *23*, 59−72.
(3) Pérez-Ramírez, J.; Kapteijn, F.; Mul, G.; Moulijn, J. A. *Appl. Catal., B* **2002**, *35*, 227−234.
(4) Pieterse, J. A. Z.; Booneveld, S.; vandenBrink, R. W. *Appl. Catal., B* **2004**, *51*, 215−228.
(5) Delahay, G.; Mauvezin, M.; Coq, B.; Kieger, S. *J. Catal.* **2001**, *202*, 156−162.
(6) Coq, B.; Mauvezin, M.; Delahay, G.; Butet, J. B.; Kieger, S. *Appl. Catal., B* **2000**, *27*, 193−198.
(7) Mauvezin, M.; Delahay, G.; Kißlich, F.; Coq, B.; Kieger, S. *Catal. Lett.* **1999**, *62*, 41−44.
(8) Pérez-Ramírez, J.; Kapteijn, F.; Mul, G.; Moulijn, J. A. *J. Catal.* **2002**, *208*, 211−223.
(9) Kaucký, D.; Sobalík, Z.; Schwarze, M.; Vondrová, A.; Wichterlová, B. *J. Catal.* **2006**, *238*, 293−300.
(10) Guzmán-Vargas, A.; Delahay, G.; Coq, B. *Appl. Catal., B* **2003**, *42*, 369−379.
(11) Kögel, M.; Mönnig, R.; Schwieger, W.; Tissler, A.; Turek, T. *J. Catal.* **1999**, *182*, 470−478.
(12) Li, L. D.; Shen, Q.; Li, J. J.; Hao, Z. P.; Xu, Z. P.; Max Lu, G. Q. *Appl. Catal., A* **2008**, *344*, 131−141.
(13) Aika, K. I.; Oshihara, K. *Catal. Today* **1996**, *29*, 123−126.
(14) Louis-Rose, I.; Méthivier, C.; Védrine, J. C.; Pradier, C. M. *Appl. Catal., B* **2006**, *62*, 1−11.
(15) Zhang, X. Y.; Shen, Q.; He, C.; Ma, C. Y.; Cheng, J.; Hao, Z. P. *Catal. Commun.* **2012**, *18*, 151−155.
(16) Shen, Q.; Li, L. D.; He, C.; Tian, H.; Hao, Z. P.; Xu, Z. P. *Appl. Catal., B* **2009**, *91*, 262−268.
(17) Panov, G. I.; Kharitonov, A.; Sobolev, V. I. *Appl. Catal., A* **1993**, *98*, 1−20.
(18) Yoshida, M.; Nobukawa, T.; Ito, S.; Tomishige, K.; Kunimori, K. *J. Catal.* **2004**, *223*, 454−464.
(19) Xie, S.; Lunsford, J. H. *Appl. Catal., A* **1999**, *188*, 137−144.
(20) Jíša, K.; Nováková, J.; Schwarze, M.; Vondrová, A.; Sklenák, S.; Sobalik, Z. *J. Catal.* **2009**, *262*, 27−34.
(21) El-Malki, E. M.; van Santen, R. A.; Sachtler, W. M. H. *Microporous Mesoporous Mater.* **2000**, *35*−*36*, 235−244.
(22) Grubert, G.; Hudson, M. J.; Joyner, R. W.; Stockenhuber, M. *J. Catal.* **2000**, *196*, 126−133.
(23) Coq, B.; Mauvezin, M.; Delahay, G.; Kieger, S. *J. Catal.* **2000**, *195*, 298−303.
(24) Nobukawa, T.; Yoshida, M.; Kameoka, S.; Ito, S.; Tomishige, K.; Kunimori, K. *J. Phys. Chem. B* **2004**, *108*, 4071−4079.
(25) Long, R. Q.; Yang, R. T. *J. Catal.* **2000**, *194*, 80−90.
(26) Qi, G.; Yang, R. T. *Appl. Catal., A* **2005**, *287*, 25−33.
(27) Amores, J. M. G.; Escribano, V. S.; Ramis, G.; Busca, G. *Appl. Catal., B* **1997**, *13*, 45−58.
(28) Ramis, G.; Yi, L.; Busca, G.; Turco, M.; Kotur, E.; Willey, R. J. *J. Catal.* **1995**, *157*, 523−535.
(29) Lin, S. D.; Gluhoi, A. C.; Nieuwenhuys, B. E. *Catal. Today* **2004**, *90*, 3−14.
(30) Műslehiddinoğlu, J.; Albert Vannice, M. *J. Catal.* **2003**, *217*, 442−456.
(31) Hadjiivanov, K. I. *Catal. Rev.* **2000**, *42*, 71−144.
(32) Underwood, G. M.; Miller, T. M.; Grassian, V. H. *J. Phys. Chem. A* **1999**, *103*, 6184−6190.
(33) Venkov, T.; Hadjiivanov, K.; Klissurski, D. *Phys. Chem. Chem. Phys.* **2002**, *4*, 2443−2448.
(34) Schwidder, M.; Heikensa, S.; Toni, A. D.; Geisler, S.; Berndtb, M.; Brückner, A.; Grünert, W. *J. Catal.* **2008**, *259*, 96−103.
(35) Long, R. Q.; Yang, R. T. *J. Catal.* **2007**, *207*, 224−231.
(36) Grossale, A.; Nova, I.; Tronconi, E.; Chatterjee, D.; Weibel, M. *J. Catal.* **2008**, *256*, 312−322.